August 2000 • NREL/SR-520-28786

Subcontractor Report

Thin Film CIGS Photovoltaic Technology

Annual Technical Report, Phase II
16 April 1999—15 April 2000

A.E. Delahoy, J. Bruns, A. Ruppert, M. Akhtar, L. Chen, and Z.J. Kiss
Energy Photovoltaics, Inc.
Princeton, New Jersey

National Renewable Energy Laboratory

1617 Cole Boulevard
Golden, Colorado 80401-3393

NREL is a U.S. Department of Energy Laboratory
Operated by Midwest Research Institute • Battelle • Bechtel

Contract No. DE-AC36-99-GO10337

August 2000 • NREL/SR-520-28786

Thin Film CIGS Photovoltaic Technology

Annual Technical Report, Phase II
16 April 1999—15 April 2000

A.E. Delahoy, J. Bruns, A. Ruppert, M. Akhtar, L. Chen, and Z.J. Kiss
Energy Photovoltaics, Inc.
Princeton, New Jersey

NREL Technical Monitor: H.S. Ullal

Prepared under Subcontract No. ZAK-8-17619-21

National Renewable Energy Laboratory

1617 Cole Boulevard
Golden, Colorado 80401-3393

NREL is a U.S. Department of Energy Laboratory
Operated by Midwest Research Institute • Battelle • Bechtel

Contract No. DE-AC36-99-GO10337

NOTICE

Available electronically at http://www.doe.gov/bridge

Available for a processing fee to U.S. Department of Energy
and its contractors, in paper, from:

U.S. Department of Energy
Office of Scientific and Technical Information
P.O. Box 62
Oak Ridge, TN 37831-0062
phone: 865.576.8401
fax: 865.576.5728
email: reports@adonis.osti.gov

Available for sale to the public, in paper, from:

U.S. Department of Commerce
National Technical Information Service
5285 Port Royal Road
Springfield, VA 22161
phone: 800.553.6847
fax: 703.605.6900
email: orders@ntis.fedworld.gov
online ordering: http://www.ntis.gov/ordering.htm

Printed on paper containing at least 50% wastepaper, including 20% postconsumer waste

Preface

Energy Photovoltaics, Inc. (EPV) has been engaged in the research and development of thin-film $CuInSe_2$ (CIS) and $Cu(In,Ga)Se_2$ (CIGS) PV manufacturing technology since 1991. During its previous 3-year research subcontract that ended in April 1998, EPV demonstrated a 9.7% CIGS minimodule and a 7.6%, 3100 cm^2, unencapsulated CIGS module that produced 24 watts. EPV's approach to CIGS production may be characterized by the following descriptors: vacuum-based, glass substrate, novel source technology, high voltage cells, safety. These characteristics permit EPV to offer uniform, defect-free films; low substrate cost; reduced materials cost; reduced resistive losses; and production without major hazards. These features will translate to a reduced manufacturing cost.

EPV's manufacturing prowess may be gauged by examining its production of tandem junction, amorphous silicon PV modules. Under a multi-year, multi-megawatt contract with SMUD, these 40 watt, 0.79 m^2 modules are being delivered at a selling price of \$1.75 - \$2/W_p with no subsidies. The modules are listed by Underwriters Laboratories Inc. (UL). The main production is by DUNASOLAR in Hungary, a plant using equipment and technology supplied by EPV. The current production level is 200kW/month. Specialty, building-integrated PV modules (BIPV) have also been manufactured in a triple-laminate format and were installed as a replacement for spandrel glass on the south and east facades of the Conde Nast building at Four Times Square, NY.

The new subcontract is entitled "Thin-Film CIGS Photovoltaic Technology." The subcontract is part of the **NREL Thin-Film Partnership Program**, and EPV participates in the National CIS Team Meetings. The objective of this subcontract (ZAK-8-17619-21) is to demonstrate the control needed to reliably produce CIGS modules with powers in the 40 - 50 watt range for a substrate size of 4300 cm^2. In addition, the deposition processes need to be fast enough to be compatible with high throughput manufacturing. During Phase I of this subcontract, EPV produced a 34 cm^2, 16-cell CIGS minimodule using its *FORNAX* process with V_{oc} 9.58V, I_{sc} 52.0 mA, FF 69.8%, and efficiency of 10.2%. This document reports progress made during the second phase (April 16, 1999 - April 15, 2000) of this three-phase, cost-shared subcontract with NREL.

Table of Contents

List of Figures

List of Tables

Introduction

Thin film photovoltaic modules based on $Cu(In,Ga)Se_2$ and related alloys have been shown to possess attributes that should enable them to compete effectively with modules based on crystalline silicon. In due course, these attributes will allow realization of a lower $\$/W_p$ cost figure for CIGS compared to crystalline Si. These attributes are stability, reliability, high efficiency, and low materials cost. The cost reduction and reliability of thin films result from monolithic integration. Monolithic integration of thin films requires fewer processing steps, and avoids the expense of crystal growing and wafering, the handling of a large number of fragile wafers, and their discrete interconnection.

For current PV module manufacturing technology it is known that the energy payback time (defined as the module deployment time required to generate the gross energy used in its manufacture) is considerably less than the expected module lifetime. The energy payback time has been calculated to be 1.8 years for thin film CIGS compared to 3.3 years for single-crystal silicon [1].

The introduction of commercially available modules based on CIS on glass substrates by Siemens Solar Industries, Camarillo, CA is a significant milestone for thin film PV, and an indication that a technology base for CIS has been established. The CIS is formed by sputtering of metals, followed by non-vacuum selenization and sulfurization using hydrogen selenide and hydrogen sulfide gases.

A new world-record thin-film solar cell efficiency (18.8% for 0.44 cm^2) was achieved by NREL using vacuum-deposited CIGS on December 28, 1998 [2]. The deposition employs four point sources and flux integration for process control. However, no group in the US has fabricated a large and efficient module using the NREL 3-stage process because of the difficulties facing scale-up of this process and the lack of off-the-shelf evaporative sources suitable for large area coating.

To overcome the manufacturing barriers confronting all-vacuum processing, Energy Photovoltaics, Inc. has developed vacuum equipment incorporating novel *linear evaporation sources* designed for uniform coating of large substrates. In addition, the equipment is capable of handling glass at the high temperatures necessary to produce the highest quality CIGS material *without glass warpage*. EPV's use of elemental selenium avoids the use of gaseous hydrogen selenide and provides for a *safe manufacturing environment*.

EPV has continued to refine the Cu linear source and other sources installed in its 0.43 m^2 pilot line. The versatility of this equipment is such that EPV can now implement almost any vacuum-based CIGS process, including its own *FORNAX* process [3], and the NREL *3-stage* process. Provided all interested parties stay the course, a glass-based, all-vacuum CIGS technology capable of producing the highest quality CIGS will move into the manufacturing arena during the next couple of years.

1.0 Molybdenum Process Development

This section discusses the development of the Mo back electrode as produced by in-line, planar magnetron sputtering on EPV's 0.43 m^2 pilot line. The process variables include glass cleaning, type and number of layers, sputtering power (W), power mode (pulse or DC), Ar pressure (mTorr), scan speed (cm/s), system base pressure, and number of pumps.

At the end of Phase I, the Mo sheet resistance was 1.3 Ω/sq, a value whose impact on module fill factor, although small, was not negligible and was felt to be avoidable. In addition, while the Mo/glass adhesion appeared satisfactory after deposition, adhesion failure was sometimes observed during later module processing. During Phase II, both additional limitations and the variability of the Mo layer were discovered, and several steps were successfully taken to rectify the situation.

In the first quarter of Phase II, the adhesion of the back electrode to the glass was improved through use of an underlayer. This in turn permitted adjustment of sputtering parameters to lower the sheet resistance to the range 0.25 – 0.4 Ω/sq without loss of adhesion. A single layer of Mo was used, and the overall back electrode thickness was 0.6μm.

In the second quarter, the crucial influence of the back contact was demonstrated by the following experiments. Samples of EPV's standard (although several months old) Mo/glass substrates were sent to NREL and were run side-by-side in CIGS depositions with the then-standard Mo used by NREL for high efficiency CIGS devices. The results were startling. The best cell efficiency on NREL-used Mo was 16%, compared to 8% using EPV-supplied Mo. A similar result was obtained in three separate runs. XRD data on the two types of Mo yielded FWHM values of 0.24 and 0.73 degrees, respectively, suggesting the EPV Mo had a smaller grain size.

An on-going concern is glass cleanliness, as tape tests sometimes result in pinholes in the Mo. Sometimes, even right after deposition, light transmission through pinholes in the Mo can be seen in certain regions of the plate. This presumably arises from dust accumulation after washing of the glass and prior to Mo deposition. It should be preventable by appropriate storage of the washed plates.

A Mo deposition was performed in a non-scanned (static) mode in order to investigate whether the Mo resistivity is a function of position, in particular whether the resistivity changes directly under the racetrack. This effect is seen strongly for ZnO [4]. Thickness and resistivity data are shown below. Unfortunately, the plate cracked due to uneven heating, causing the four-point probe readings to artificially rise in the neighborhood of the break. The two lines marked "trace" represent the locations of the racetrack. There is a possible slight rise in resistivity at these locations, but no definite conclusion can be drawn. A shorter deposition may be attempted.

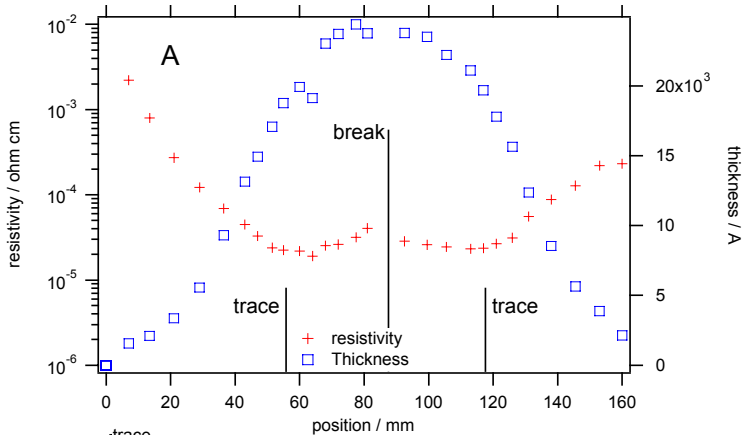

Figure 1.1 Thickness and resistivity of Mo sputtered in a static mode

In the third quarter of Phase II the Mo recipe was again modified, and included changes to the underlayer, and re-adoption of bi-layer Mo. The power was supplied in pulse mode. This recipe again gave low sheet resistance (0.2 – 0.3 Ω/sq) and good adhesion. The average Mo resistivity was 12.6 μΩ cm (the bulk value being 5.2 μΩ cm). Samples of this Mo cut from a single substrate with and without the underlayer (#Mo 91) were sent to NREL (Miguel Contreras) for CIGS deposition alongside NREL-produced Mo. Table 1.1 summarizes the PV parameters of the three best cells on each of the three substrates that were simultaneously coated with CIGS in run C1256 at T_s = 600°C. All cells were 0.43 cm^2 in area and had no AR coating.

Table 1.1 PV parameters for NREL CIGS cells C1256-1 on EPV Mo (Mo 91 with underlayer), C1256-2 on NREL Mo, and C1256-3 on EPV Mo (Mo 91 without underlayer)

Substr. #	Mo	Cell	V_{oc} (V)	J_{sc} (mA cm^{-2})	I_{sc} (mA)	FF (%)	Eff (%)	V_{mp} (V)	I_{mp} (mA)
1256-1	EPV	1	0.646	34.13	14.67	75.87	16.7	0.530	31.55
		2	0.644	35.67	15.34	74.68	17.2	0.530	32.37
		3	0.640	35.17	15.12	74.85	16.8	0.530	31.78
1256-2	NREL	1	0.567	30.28	13.02	72.26	12.4	0.460	26.95
		3	0.558	30.84	13.26	71.92	12.4	0.460	26.92
		4	0.550	30.62	13.17	71.87	12.1	0.430	28.17
1256-3	EPV	1	0.575	33.18	14.27	72.50	13.8	0.450	30.76
		3	0.558	34.35	14.77	70.99	13.6	0.440	30.93
		6	0.540	35.21	15.14	70.90	13.5	0.430	31.35

The most significant conclusion, as evidenced by the 17.2% cell, is that EPV has demonstrated large area sputtering of a Mo back electrode capable of supporting very high efficiency cell processing. This is an important result.

In this run (C1256), the performance of the cells on EPV Mo with the underlayer were significantly superior to those on EPV Mo without the underlayer in terms of voltage and fill factor. And both types of EPV Mo apparently outperformed the NREL-produced Mo, most consistently in short-circuit current density.

However, similar CIGS runs were conducted on the EPV and NREL Mo substrates at substrate temperatures of 590°C and 610°C. The PV parameters of the best cell on each substrate from the three runs (at 590, 600, and 610°C) are summarized in Table 1.2.

Table 1.2 PV parameters as a function of substrate temperature and Mo type

Run-substr.	T_s (°C)	Mo	Underlayer	V_{oc} (V)	J_{sc} (mA cm^{-2})	FF (%)	Eff (%)
1255-1	590	EPV	Yes	0.593	35.86	72.87	15.5
1255-2	590	NREL		0.614	34.13	72.98	15.3
1255-3	590	EPV	No	0.641	33.94	73.72	16.0
1256-1	600	EPV	Yes	0.646	34.13	75.87	17.2
1256-2	600	NREL		0.567	30.28	72.26	12.4
1256-3	600	EPV	No	0.575	33.18	72.50	13.8
1257-1	610	EPV	Yes	0.582	35.66	71.95	14.9
1257-2	610	NREL			Grid problem		
1257-3	610	EPV	No	0.561	34.16	71.64	13.7

From this full set of data it is difficult to draw universal conclusions as to the desirability of the underlayer or the effect of substrate temperature. Consistently good results were obtained at 590°C, while the optimum T_s for this particular CIGS recipe could shift with the presence of the underlayer or with Mo type.

Having demonstrated the ability to make "high-efficiency" Mo, the following questions arose: How sensitive is the good Mo to sputtering conditions, and over what region of process space can good Mo be maintained? Can good Mo be recognized simply by its SEM signature? Have subsequent small changes to the Mo recipe preserved Mo quality or has Mo quality been compromised? From a practical point of view, the Mo process cannot be said to be under control until this larger investigation has been completed.

During the fourth quarter, steps were taken to try to attack these questions. It was decided that the sensitivity of overall Mo properties to the sputtering pressure for the 2nd Mo layer would be studied. Run 110-1 represented the starting point for these studies. For practical reasons of reducing process sensitivity to gas flow, one diffusion pump was blanked off during sputtering for the remaining runs. The run numbers, sputtering pressures and basic film properties for this series of Mo depositions are summarized in Table 1.3.

Table 1.3 Mo properties as a function of 2nd Mo layer sputtering pressure

Sample #	Mo2 pressure (mTorr)	Sheet resistance (Ω/sq.)	Thickness (μm)	Resistivity (μΩ cm)
110-1	4	0.24	0.81	19
110-2*	4	0.28	0.78	22
110-3*	6	0.22	0.77	17
110-4*	8	0.31	0.82	25
110-5*	3	0.23	0.91	21

* 1 diff pump blanked off & new underlayer parameters adopted

There is no clear correlation of properties with pressure, although it appears that the Mo exhibits a minimum in electrical resistivity at 6 mTorr.

SEM micrographs were obtained for all five films in Table 1.3. Micrographs taken at 100kX are shown in Figure 1.2 below for 2nd Mo deposition pressures of 4 and 8 mTorr.

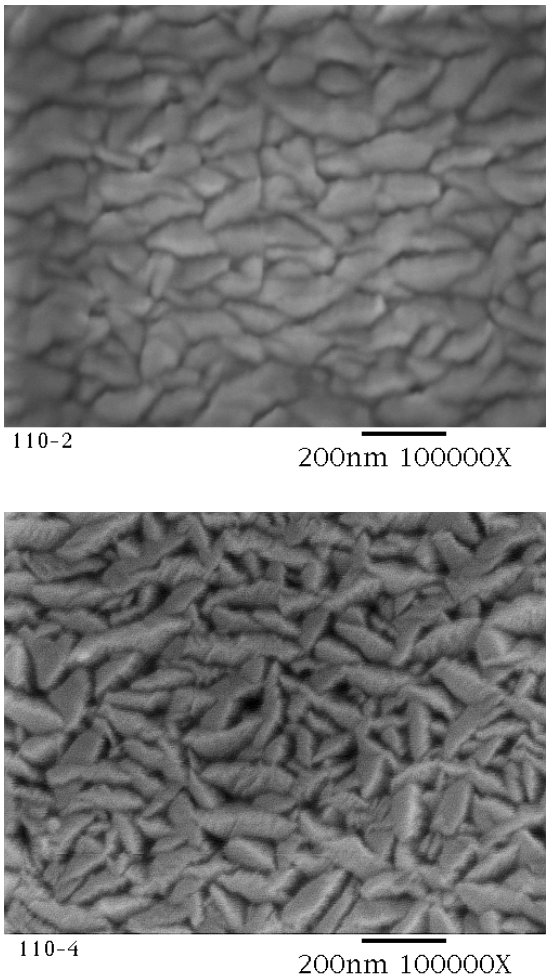

Figure 1.2 SEM micrographs of Mo back contact layers prepared at different 2nd Mo sputtering pressures

The size of the grain interstices is clearly influenced by sputtering pressure. A set of these samples were mailed to NREL for device fabrication, but were apparently lost. Thus the correlation of morphology and device performance has not yet been established. At the end of the fourth quarter, the power mode for Mo deposition was changed to DC. A new set of Mo depositions, with associated film and device analysis, is planned for the first quarter of Phase III.

2.0 Small Area CIGS

The Hercules, 4-source, R&D deposition system for CIGS is currently configured to accommodate four 2" x 4" substrates. Other stations in the R&D CIGS line are CBD CdS, buffer layer evaporation, and RF sputtered bi-layer ZnO. Devices are routinely characterized by thickness, I-V, and QE measurements. The goals for this program include:

1. Recipe development for 15% CIGS cells (no AR coating)
2. Comparative evaluation of pilot line processing
3. Supply of CIGS for alternative buffer layer deposition
4. Supply of CIGS for mini-module fabrication and diagnostics
5. Special projects, such as source material evaluation

Both 3-stage and 2-stage processing can be performed in the Hercules. Recently, good device results have been obtained using a simple 2-stage process involving Cu deposition in the first stage. For the metals Cu, In, and Ga, open boat sources are used, with Cu located in the middle. The dark and light I-V curves for a 13.3% cell produced in the R&D line in the fourth quarter of Phase II (run H-0033) are shown in Figure 2.1 below.

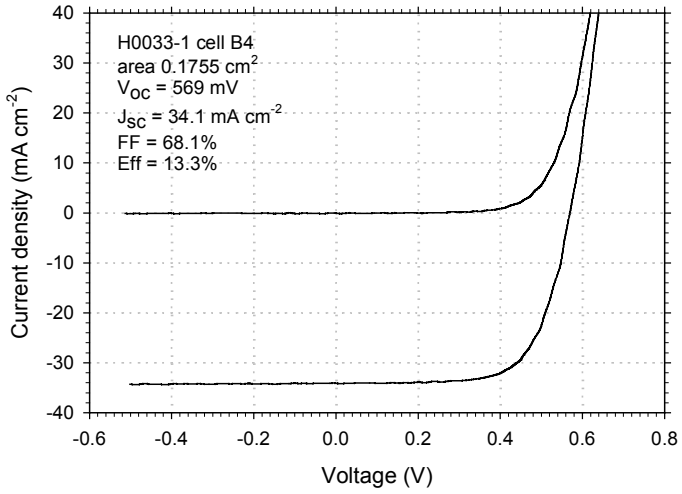

Figure 2.1 I-V curve for an R&D CIGS device with CBD CdS (ZnO:Al bilayer/CdS/CIGS).

This cell exhibited a V_{oc} of 569 mV, J_{sc} 34.1 mA/cm^2, and FF 68.1%. Fifteen cells were defined on each of the four substrates. The average V_{oc} for all 15 cells on each substrate of run H-0033 were 534, 538, 551, and 546 mV.

The spectral response of a cell from the Hercules system is shown in Figure 2.2.

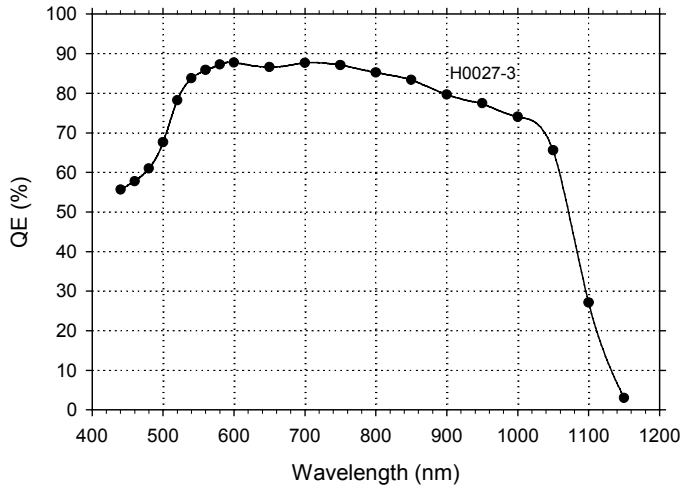

Figure 2.2 Quantum efficiency versus wavelength for an R&D CIGS cell

3.0 Junction Research

Although the standard CBD CdS process forms the best junctions, it generates a substantial volume of liquid waste, and the use of Cd raises controversial environmental and health concerns. Our long term objective is to replace CBD CdS by a dry, Cd-free process capable of in-line implementation after CIGS deposition. Ultimately the device yield and efficiency should be comparable to CBD CdS. The simplest approach would be in-line evaporation of a single material directly onto the freshly formed CIGS. Since Cd and Zn are known n-type dopants in CIS, it could be advantageous for the buffer layer to contain one of these elements to form a shallow n-p homojunction in the absorber, see for example [5]. Furthermore, since In and Se are already present in CIS or CIGS, we contemplated the use of $ZnIn_xSe_y$ (ZIS) as a buffer material. This material was first applied to CIGS by another technique, namely three-source co-evaporation of the elements Zn, In, and Se, by Konagai et al. [6,7]. At sufficiently high substrate temperatures the defect chalcopyrite (thiogallate) $ZnIn_2Se_4$ was obtained. The bandgap of this material is reported to be 2.0eV [8]. In distinction to this work, we proposed to synthesize $ZnIn_2Se_4$ (and related materials) from the elements as a bulk material, and to use it as a single evaporation source material for buffer layer deposition in order to simplify ZIS film formation.

Bulk synthesis of $ZnIn_2Se_4$ (ZIS) was conducted by intermixing of Zn and In in appropriate atomic fractions, followed by reaction with Se at elevated temperatures. The resulting material was ground to granular form. XRD analysis of the material demonstrated the presence of $ZnIn_2Se_4$, together with secondary phases of $Zn_{0.4}In_2Se_{3.4}$, In_2Se_3, and InSe. The XRD spectrum is shown in Figure 3.1 below, with the (112) peak of $ZnIn_2Se_4$ clearly seen.

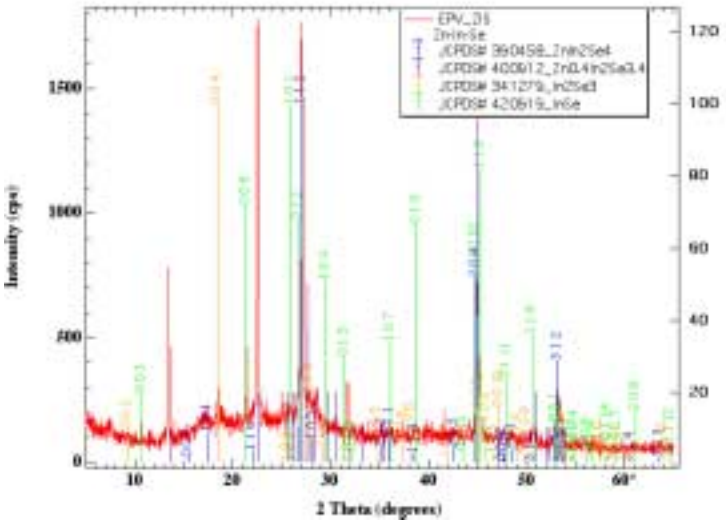

Figure 3.1 X-ray diffraction pattern of granular ZIS ($ZnIn_2Se_4$) source material.

The bulk $ZnIn_2Se_4$ material prepared at EPV was evaluated as a source material. The ZIS was loaded into an open tungsten boat and evaporated onto glass, glass/Mo, and Mo planar gap cells. It was found to sublime, and therefore could be successfully employed as an evaporation source. An Auger depth profile of the film resulting from complete evaporation of a charge is shown in Figure 3.2 below.

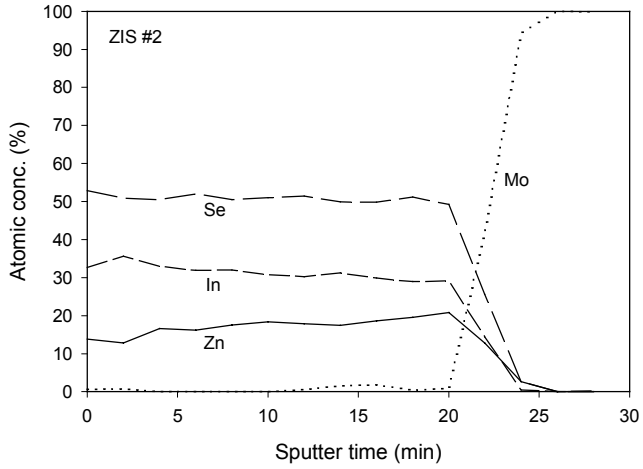

Figure 3.2 Auger depth profile of ZIS film obtained by evaporation of a charge of ZIS source material to completion.

It can be seen that all three elements are present in the film at all depths. (Since NREL does not possess a suitable standard for this material, the atomic concentrations cannot be regarded as absolute.) It appeared that the In/Zn ratio increased somewhat during deposition of the $ZnIn_xSe_y$ film.

ZIS films were deposited over a range of substrate temperatures and characterized according to composition, bandgap, and conductivity. First, $ZnIn_xSe_y$ thin films were deposited on glass at three different substrate temperatures T_s – room temperature (RT), 230°C, and 300°C. In each run, 2g of fresh source material were degassed and evaporated slowly to completion. Table 3.1 shows the variation in thickness, and qualitative elemental concentrations as determined by EDS.

Table 3.1. Change of ZIS film thickness and qualitative composition with deposition temperature

ZIS T_s (°C)	Thickness (A)	Zn	In	Se
RT	5250	0.23	0.37	0.40
230	4200	0.12	0.40	0.48
300	3900	0.10	0.38	0.53

The decline in thickness as the substrate temperature T_s was raised implies a reduced sticking coefficient. The trend towards lower Zn fraction at higher T_s suggests a reduced Zn incorporation. Also apparent is a reduction in Se fraction at lower T_s, consistent with the secondary phases that contain less Se and the metallic In inclusions seen in the XRD data for these films (Figure 3.3).

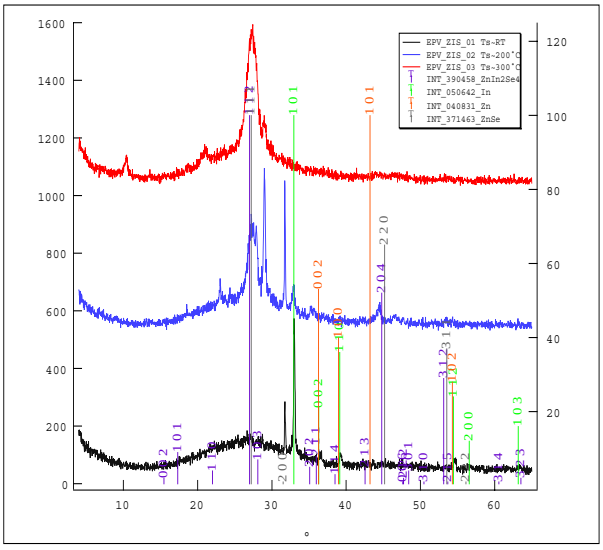

Figure 3.3 XRD pattern of ZIS films deposited at substrate temperatures of 30, 230, and 300°C.

The total reflectance and transmittance spectra from 400 nm to 1400 nm were obtained for these films. The RT sample exhibits a flat reflectivity and almost zero transmittance, essentially metallic behavior. The T_s = 300°C sample exhibits dielectric behavior in the IR, while the 230°C sample behaves intermediately with IR absorption. For the better-behaved 300°C sample, the absorptance (energy absorbed divided by energy in) was calculated from the expression

$$A = (1\text{-}R\text{-}T)/(1\text{-}R) = 1 - T/(1\text{-}R)$$

The absorption coefficient $\alpha(\lambda)$ was then calculated from: $T/(1\text{-}R) = \exp(-\alpha t)$ where t is the film thickness. The absorption coefficient α for an allowed direct transition varies with photon energy $h\nu$ according to [9]:

$$(\alpha h\nu)^2 \sim (h\nu - E_g)$$

If the absorption data for the 300°C sample are analyzed as though the film were a single phase material with direct absorption, then a plot of $(\alpha h\nu)^2$ vs. $h\nu$ yields a bandgap E_g for the material of 1.9 – 2.0eV. This plot is shown in Figure 3.4 below.

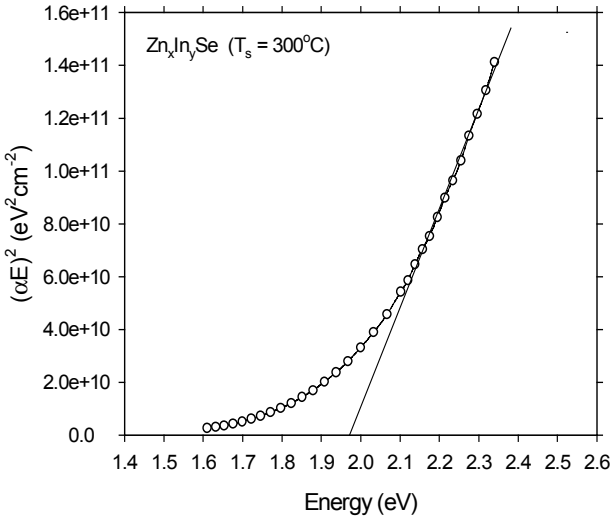

Figure 3.4 Plot of $(\alpha h\nu)^2$ vs. $h\nu$ for a ZIS film deposited at T_s = 300°C.

For film thicknesses of around 0.5μm, reasonable properties were obtained for T_s = 270-300°C: the dark conductivity σ_d was 1.5 x 10^{-4} $(\Omega\ cm)^{-1}$, and the photoconductivity σ_{ph} was 4.9 x 10^{-4} $(\Omega\ cm)^{-1}$ (as measured under white light at 1 sun irradiance). Dark and light currents were measured using a Keithley model 485 picoammeter for an applied voltage of 40V across a planar gap of a few mm. The dark conductivity decreased with decreasing film thickness.

EPV has explored several possible material compositions as possible ternary buffer layers, with variable device results. Thus, another candidate material is $ZnGa_xSe_y$ (ZGS). Thicker films of this material appear yellow-gold compared to the brownish red of ZIS, and clearly have a higher bandgap. However, the material appears too resistive for devices, and the photocurrent is suppressed. With a thin ZGS/ZIS bilayer an 8.1% cell was obtained, although the device suffered from dark-light crossover (see Figure 3.5).

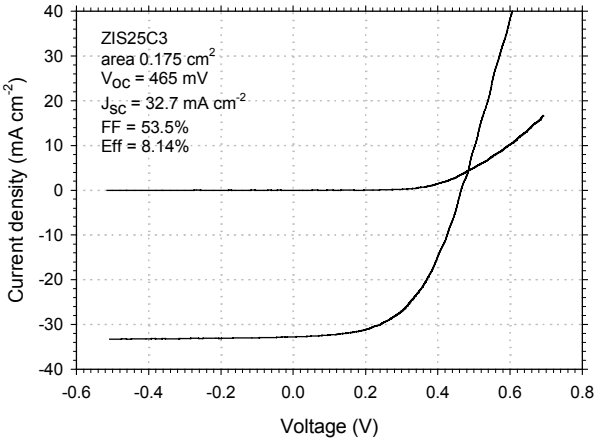

Figure 3.5 Dark and light I-V curves for a ZnO:Al/ZGS/ZIS/CIGS device showing crossover.

Other ternary compositions have been tried ranging from In_2Se_3:Zn to ZnSe:In. One material has proved promising and consistently provides reasonable cell efficiencies. Using this material, designated "ZIS", as a buffer layer in the configuration ZnO:Al/ZIS/CIGS/Mo/glass, a number of cells were prepared. Figure 3.6 shows the variation of short-circuit current density J_{sc} with the mass of ZIS evaporated.

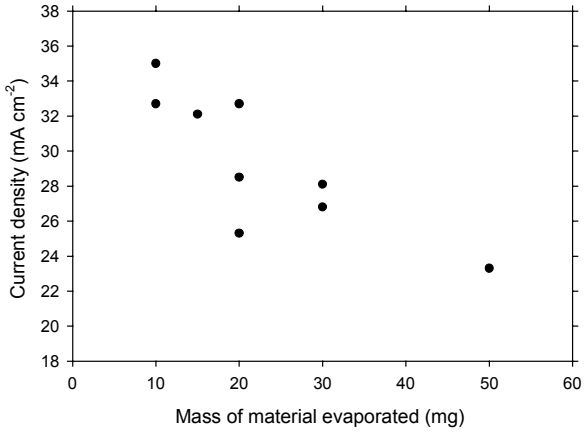

Figure 3.6 Solar cell short-circuit current density versus mass of ZIS evaporated.

(Film thicknesses cannot be extrapolated from the T_s studies using 2g ZIS since a reduced source-substrate distance was used for devices.) Reduction of the ZIS thickness allowed J_{sc}'s of up to 35 mA cm^{-2} to be achieved.

With a relatively thin ZIS buffer layer an 11.5% cell has been achieved with V_{oc} 560 mV, J_{sc} 32.1 mA cm^{-2}, and FF 64.3% (see Figure 3.7 below) [10]. By extrapolation from the measured thickness of ZIS films using a 0.4g charge, the ZIS buffer layer in this device is estimated to be about 25nm (250A) in thickness.

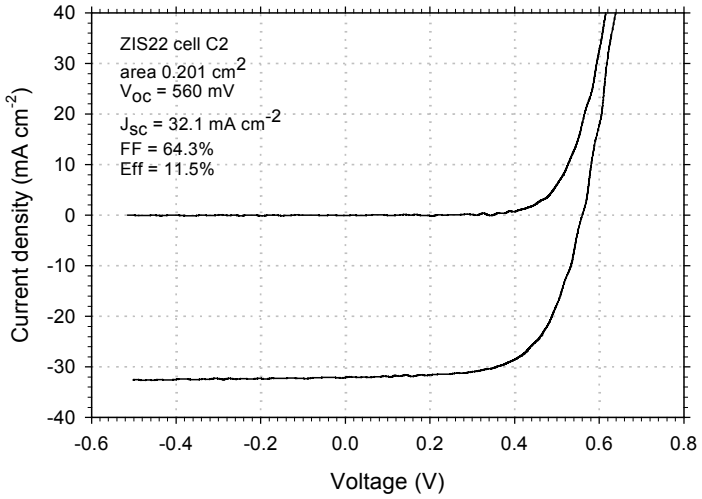

Figure 3.7 I-V curve for an 11.5% CIGS cell with vacuum-deposited, non-Cd, ternary buffer layer (ZIS) in the configuration ZnO:Al/ZIS/CIGS.

Using the preferred ZIS material, cells can be fabricated with no dark-light crossover of the I-V curve. Furthermore, no light soaking effects are seen, unlike the strong increase in V_{oc} exhibited by ZnO/CIGS devices where the ZnO is prepared by the *ROMEAO* process [11].

The spectral response of the 11.5% cell using ZIS is shown in Figure 3.8, and is compared to that of a good CIGS cell from EPV's R&D system that uses CBD CdS as the buffer layer. The ZIS cell is shown to have a superior quantum efficiency for wavelengths less than 520 nm. There is a suggestion of broadband absorption in the ZIS cell, but this remains to be confirmed and its origin (ZnO, ZIS, or CIGS) determined.

At the time of writing, the efficiency of CIGS cells with evaporated ZIS buffer layers is in general only 70-80% of that of cells with CBD CdS buffer layers. However, the CIGS quality, substrate temperature and some other ZIS deposition parameters remain to be optimized. In this way we hope to approach the performance of the 15.1% cell achieved by co-evaporation of ZIS [7].

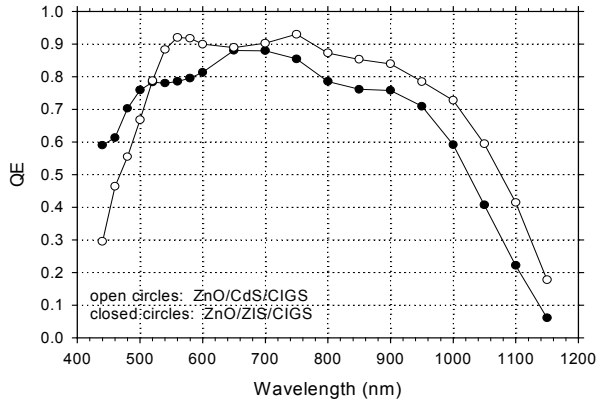

Figure 3.8 Spectral response for CIGS cells (of different bandgap) with CdS and ZIS buffer layers.

An expanded effort on ZIS will be mounted via the EPV Sub-team of the National CIS R&D Team. The team members are: Miguel Contreras, NREL; Alan Delahoy, EPV; Don Morel, USF; Larry Olsen, WSU.

4.0 Large Area CIGS

To prepare CIGS over a large area (currently 0.43 m^2) EPV delivers materials from a sequential arrangement of line sources to a heated substrate that is translated in a direction perpendicular to the axes of the sources [12]. In particular, a linear evaporation source for Cu delivery has been developed. This technological "tour de force" allows EPV to build large area CIGS systems possessing considerable process flexibility, and capable of implementing either the EPV *FORNAX* process [3], or the NREL 3-stage process using elemental sources. The evaporated material is delivered downwards onto the substrate over a coating width of 45 cm.

Similar in-line evaporation has been reported by the group at ZSW [13], with downward-facing line sources mentioned in reference [14]. GSI is now operating systems for deposition onto 16.5 cm and 33 cm web substrates [15]. The IEC group has also recently constructed an in-line evaporation system (designed for upwards evaporation), and has reported data pertaining to the substrate passing sources in the sequence Cu, Ga, In [16]. Good thickness uniformity was demonstrated over a width of 15cm. The ZSW, GSI, and IEC groups have reported a homogeneous distribution of copper throughout the thickness of the film (implying a high mobility for Cu atoms), but a graded distribution of In and Ga at their respective substrate temperatures as predicted by flux models for a single pass of the substrate. GSI found that source arrangement and sequencing profoundly affected CIGS composition, adhesion, density, and morphology when depositing onto polyimide,

but had a smaller influence for depositions onto stainless steel because of the higher substrate temperature and enhanced diffusion.

The figure below shows the thickness distributions of (In,Ga)Se_x and CIGS films prepared in the EPV CIGS pilot line across the width of the glass substrate i.e. in the direction of the source axes. Good uniformity is obtained over a coating width of 45 cm.

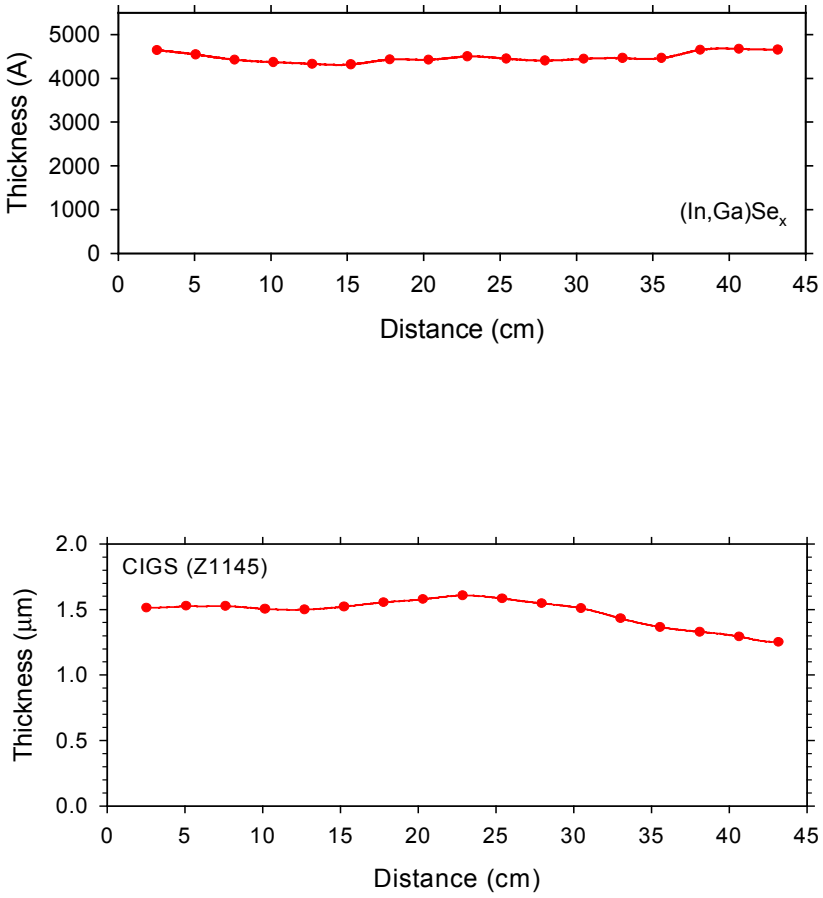

Figure 4.1 Thickness distributions for (In,Ga)Se_x and CIGS in the direction of the linear sources

To monitor the quality of CIGS prepared in the pilot line, small sections of the substrate are processed through the R&D scale CdS/ZnO stations. Figure 4.2 shows the I-V curve of a 12.0% cell with 581 mV V_{oc} prepared using pilot line CIGS. This result demonstrates that high quality CIGS can be prepared by in-line, linear source evaporation.

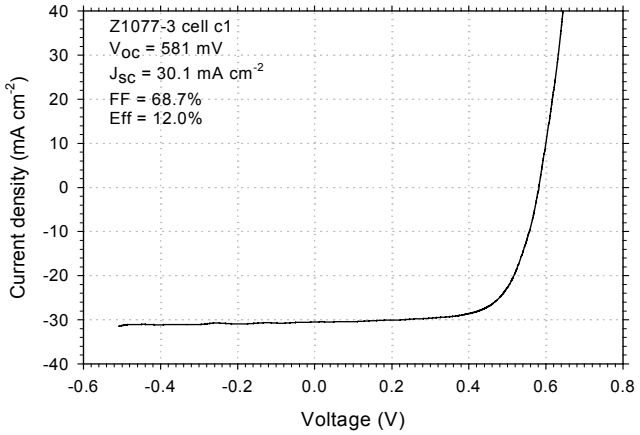

Figure 4.2 I-V curve for 12.0% cell prepared using pilot line CIGS

Following deposition of CIGS onto laser-scribed Mo on 0.43m^2 glass plates, interconnected modules were prepared using the usual process sequence (CBD CdS, mechanical scribing for patterning step #2, ZnO:Al deposition by sputtering, mechanical scribing for patterning step #3). A variety of routine diagnostic tests have been instituted in order to quantify the quality and performance of the pilot line CIGS, the device structure on the plate, and the overall module. These are:

1. Processing of 2" x 4" CIGS cut ups through the R&D CdS and ZnO stations
2. Segment V_{oc} map across module
3. Full module I-V curve
4. Delineation/measurement of diagnostic cells on left and right sides of plate

An example of these test procedures (#1 from the list above) is given in Figure 4.3 below, which shows the PV parameters for cells made on 2" x 4" pieces cut from a 0.43 m^2 plate after processing through the R&D CdS and ZnO stations.

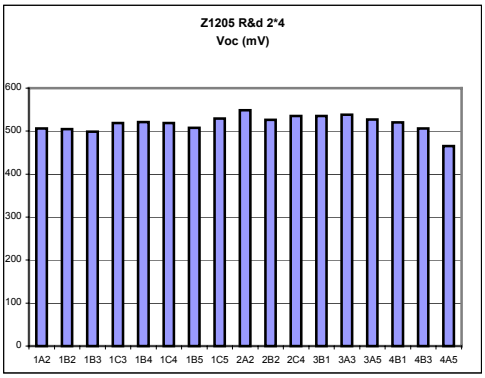

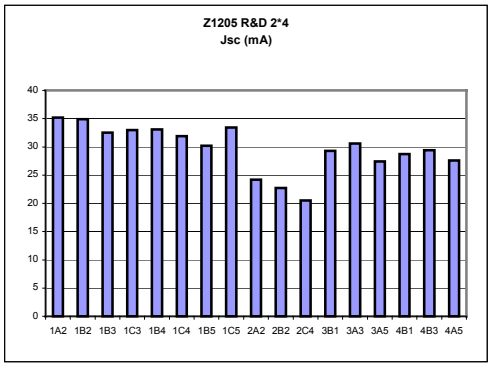

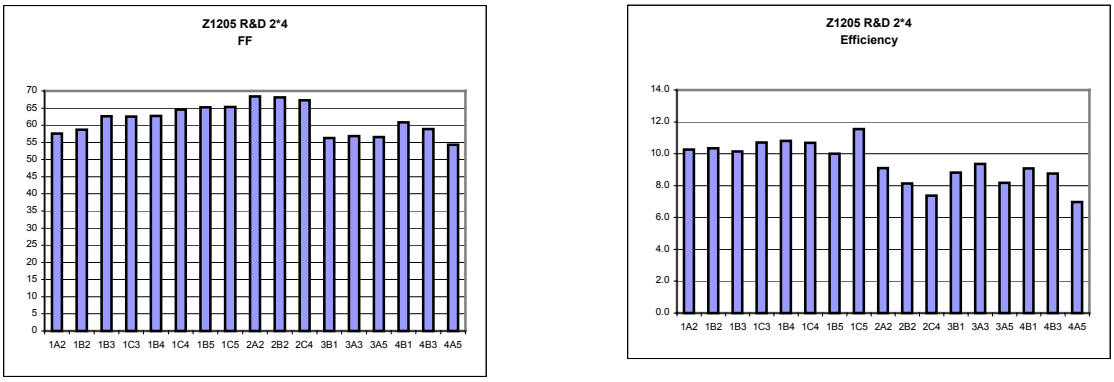

Figure 4.3 Data from pilot line CIGS cut-ups after processing through R&D line

These data show the CIGS to be of good quality and capable of producing a cell V_{oc} of about 500-530 mV, a J_{sc} of 30-35 mA/cm^2, FF of 60-65%, and efficiency of 9-11%. A noticeable dip in J_{sc} is seen in some cells, and this needs to be diagnosed. Data such as these are then compared to data obtained on diagnostic cells prepared on the actual large CIGS plate, from which information concerning the relative quality and control of the pilot line CdS and ZnO versus R&D line CdS and ZnO can be obtained.

Other activities related to CIGS deposition and module fabrication and diagnostics have included:

1. reliability of source temperature measurement
2. increase of plate travel distance
3. thermal management in the pilot line system
4. reliability of laser isolation of Mo
5. a study of storage time effects (CIGS - CdS, and CdS - ZnO)
6. improved operator training for mechanical scribing
7. CIGS laser scribing studies
8. CdS reproducibility
9. re-optimization of sputtered ZnO:Al
10. morphology and composition analysis of pilot line CIGS, and correlation with QE data

Here we discuss items #9 and #10 only. We have previously reported that the DC sputtering process using ceramic targets for large area ZnO:Al needs to be periodically optimized as the target is eroded. In this last optimization, the O_2 bleed was varied while other parameters were held constant. The other parameters were: pressure 3.5 mTorr, power 2100 W (pulse mode), scan voltage 0.43V, number of scans 2. Operationally, the ratio of numbers proportional to the flows of Ar and Ar+5%O_2 was used as the parameter to be varied. The data is summarized in Table 4.1 below.

Table 4.1 Re-optimization of oxygen bleed for large area sputtered ZnO:Al

Flow ratio $Ar/(Ar+O_2)$	R_s Ω/sq	T_{IR} %	Thickness A
10	16.8	80	9300
15	13.8	76	9000
20	13.3	74	9300

The previous standard flow ratio was 15. After these experiments a flow ratio of 10 was adopted in order to benefit from the increased transmission.

Samples of CIGS material from two Zeus runs with differently performing devices were sent to NREL for analysis in order to try to understand the reasons for the difference. The run numbers were Z1129 and Z1140. The small Z1129 piece was carried on a standard glass substrate (and subsequently processed through the R&D line with devices), and produced a current density of about 27 mA/cm^2, while the Z1140 piece was cut from a completed submodule and was selected because of its abnormally low current density of 16.4 mA/cm^2. The quoted current densities were derived from integration of the product of the QE and AM1.5 spectra. The film thickness for Z1129 was 1.5 μm, and the device efficiency was 8.9%.

SEM micrographs (see Figure 4.4 below) reveal significant differences in morphology. The low current sample Z1140 shows evidence of platelet or striated growth that is absent in the higher current sample Z1129. This platelet growth morphology is apparently associated with low current density. The tiny bumps on the grains of Z1129 (measles) do not appear in normal high quality CIGS. Their origin and impact on efficiency is unknown.

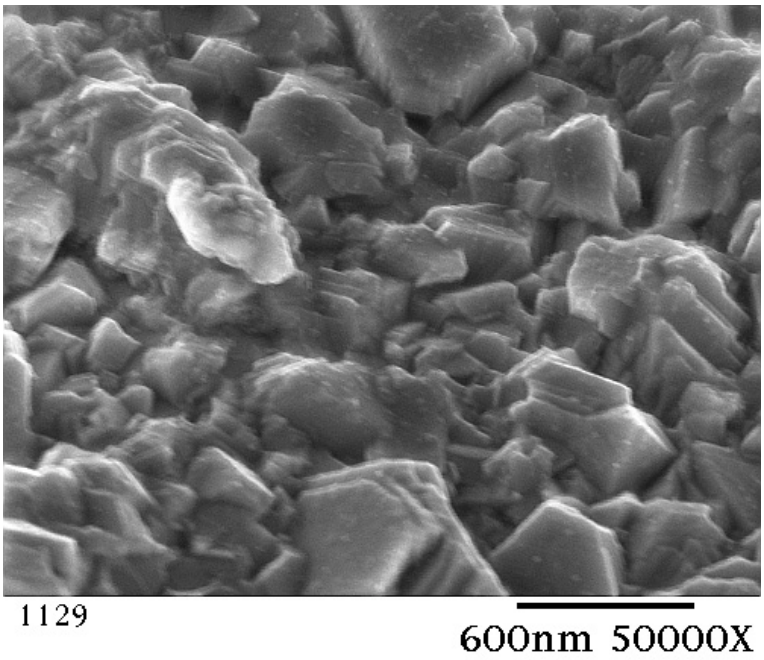

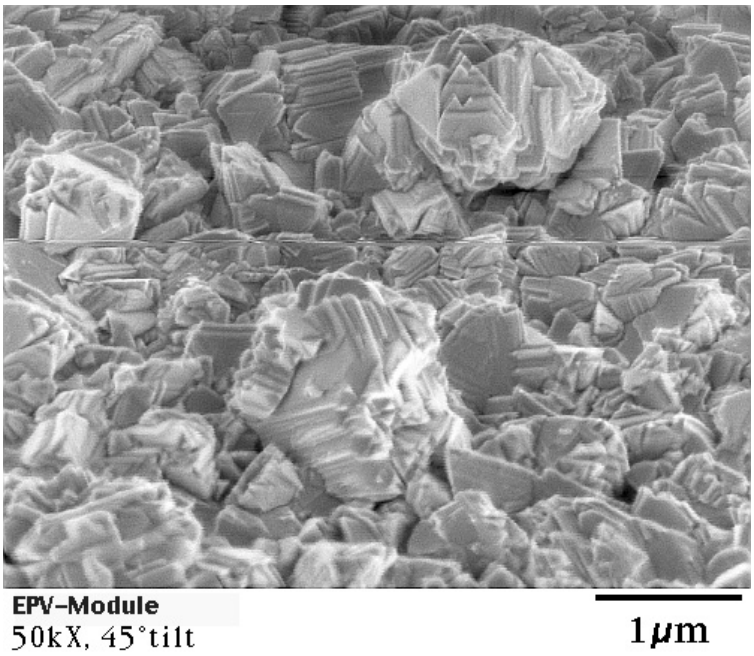

Figure 4.4 SEM micrographs of pilot line CIGS from runs Z1129 and Z1140

The composition of the CIGS in these two runs was determined by ICP (Inductively Coupled Plasma) analysis at NREL. For the submodule, the composition was measured at four positions along a line running perpendicularly to the scribes i.e. along the axis of the linear sources. The data are shown in Table 4.2 below.

Table 4.2 Composition of CIGS from runs Z1129 and Z1140

Parameter	Z1129	Z1140 3"	Z1140 7"	Z1140 11"	Z1140 15"
Cu (at. %)	23.7	23.0	21.8	20.5	21.0
In (at. %)	18.7	19.1	20.6	20.4	20.3
Ga (at. %)	7.4	7.3	7.3	7.0	6.7
Se (at. %)	50.2	50.6	50.4	52.1	52.1
Cu/(In+Ga) %	90.7	87.3	78.3	75.1	77.9
Ga/(In+Ga) %	28.5	27.6	26.1	25.4	24.7

The composition of Z1129 is perfect, and entirely compatible with high efficiency CIGS. Z1140, however, with an average Cu/(In+Ga) of 79.6%, is too Cu-poor. It also exhibits gradients of Cu across the plate. The Ga/(In+Ga) distribution is satisfactory.

Depth profiles of these two runs were obtained by Auger analysis at NREL. These profiles are perfectly reasonable, and prove that EPV's large area CIGS process and equipment can produce films of uniform composition in depth. The profile of Z1140 shows constant concentrations of all four elements Cu, In, Ga, Se throughout the layer. The profile of Z1129 (shown in Figure 4.5 below) exhibits a slightly increasing

concentration of Ga away from the front surface and towards the back, and a slightly decreasing profile of In.

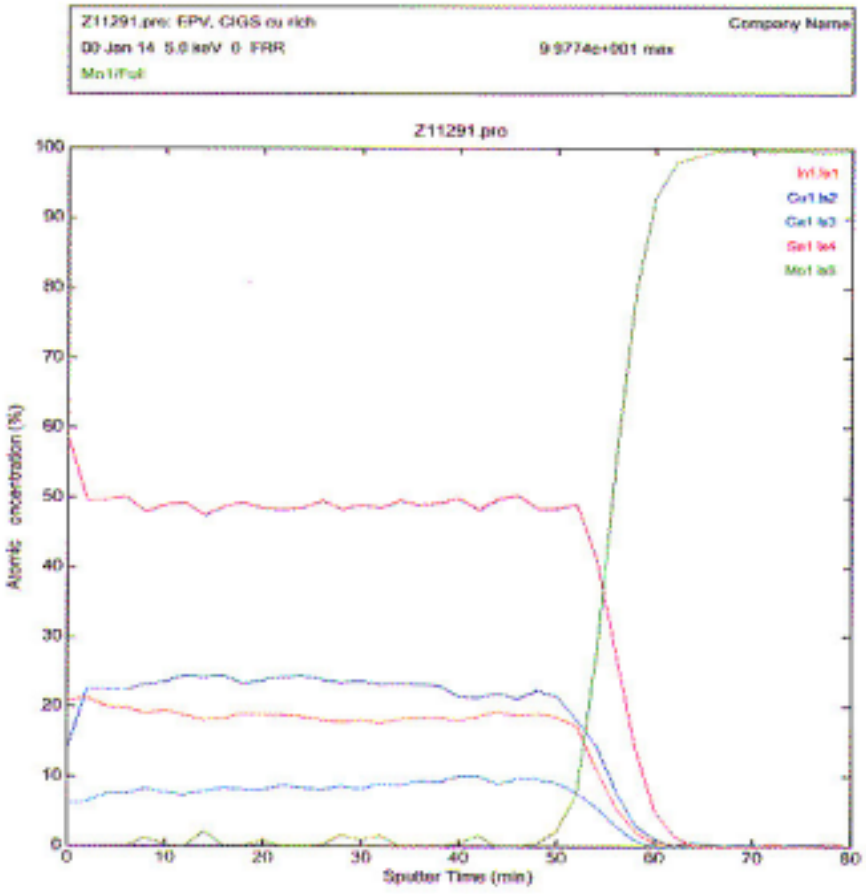

Figure 4.5 Depth profiles of Se, Cu, In, Ga, and Mo for pilot line CIGS (run Z1129)

Module results during this Phase have been disappointing. Run Z1139 gave a large area module V_{oc} of 32.1 V, FF 49.6%, but low current density. Following institution of the various diagnostic tests, module fabrication was resumed. In run Z1212, module voltages up to 36.25 V were obtained for 81 segments, corresponding to an average V_{oc}/cell of about 450 mV, a respectable result. However, module J_{sc}s were somewhat low at 25 mA/cm^2, and FF was low at about 40-43%. These results are currently being investigated.

EPV, Inc.
Thin-Film CIGS Photovoltaic Technology
Subcontract no. ZAK-8-17619-21

Phase II Summary

- EPV has demonstrated that it can sputter a Mo back contact capable of supporting very high efficiency cell processing. Using EPV Mo, NREL has deposited a 17.1% CIGS cell (no AR coating). EPV believes it can identify the signature of "good" Mo. The Mo was produced on EPV's 0.43 m^2 pilot line equipment.

- EPV has performed compound synthesis for several classes of materials, namely non-Cu precursor materials, Cu-containing materials, and ternary buffer materials. Using a ternary compound synthesized at EPV (ZIS) as an evaporation source material for the buffer layer, a Cd-free CIGS device has been produced having an efficiency of 11.5% (560 mV, 32.1 mA/cm^2, FF 64.3%). The ZIS films are photoconductive, and the devices exhibit no dark-light crossover or light soaking.

- EPV initiated the interest of the University of Oregon in capacitance spectroscopy of CIGS devices. An Urbach tail with characteristic energy E0 < 20meV was identified by transient photocapacitance spectroscopy.

- Small area CIGS devices were produced in the pilot line system with an efficiency of 12.0% (581 mV, 30.1 mA/cm^2, FF 68.7%), and in an R&D scale system with 13.3% efficiency (569 mV, 34.1 mA/cm^2, FF 68.1%).

- An improved linear evaporation source for Cu delivery has been developed and was used for CIGS formation in the pilot line system. The deposition width is 45 cm. This technological "tour de force" allows EPV to build large area CIGS systems possessing considerable flexibility. In particular, both EPV's *FORNAX* process and NREL's 3-stage process have been implemented on the pilot line. A CIGS thickness uniformity of plus/minus 7% over a 40 cm width has been achieved.

- A 4-head linear source assembly was designed, constructed, and is in use. Flux monitoring is practiced.

- Large area CIGS modules were produced with V_{oc}'s up to 36.3 V.

- EPV has started to construct an entirely new CIGS pilot line for scale up and limited manufacturing purposes. The coating width will be 65 cm.

- The company's analytical capabilities are currently being upgraded with the installation of ICP and SEM/EDS facilities.

Future Plans

During Phase III, we will continue to study the performance of various types of Mo, optimize the non-Cd, ternary buffer layer by applying it to CIGS routinely produced by a 2-stage R&D process, improve scribing and interconnects, and greatly increase efforts in lamination and stress testing. With regard to the CIGS itself we plan to monitor and optimize the Ga/(In+Ga) depth profile, add novel control methods to the linear source based CIGS machines to achieve targeted Cu/(In+Ga) ratios, and thoroughly document the CIGS composition and morphology using in-house ICP and SEM capabilities. A new initiative in laser scribing of CIGS will also be undertaken.

EPV has committed to scale up its CIGS technology and is building a new pilot line capable of coating substrates 0.79 m^2 in area. The new technology described above will be utilized in this line. Demonstration of high yields, reproducibility, and greatly increased throughput for the CIGS layer will be a major focus. In addition to upscaling experience, it is planned that limited commercial CIGS product will result from this line.

References

[1] K.E. Knapp and T.L. Jester, presented at 16th European Photovoltaic Solar Energy Conference and Exhibition, Glasgow, UK, May 1-5, 2000.

[2] M.A. Contreras, B. Egas, K. Ramanathan, J. Hiltner, A. Swartzlander, F. Hassoon, and R. Noufi, Prog. Photovolt: Res. Appl. 7, 311-316 (1999).

[3] A.E. Delahoy, D. Chorobski, F. Ziobro, Z.J. Kiss, AIP Conf. Proc. Vol. 462 (AIP, NY, 1999) 144-151.

[4] A.E. Delahoy and M. Cherny, Proc. MRS, Vol. 426 (1996) p. 467.

[5] K. Ramanathan, H. Wiesner, S. Asher, D. Niles, R.N. Bhattacharya, J. Keane, M.A. Contreras, and R. Noufi, Proc. 2nd World Conf. And Exhibition on Photovoltaic Solar Energy Conversion 1998, p. 477.

[6] M. Konagai, Y. Ohtake, and T. Okamoto, MRS Symp. Proc. Vol. 426 (1996) 153-163.

[7] A. Yamada, S. Chaisitsak, Y. Ohtake, M. Konagai, Proc. 2nd World Conf. And Exhibition on Photovoltaic Solar Energy Conversion 1998, p. 1177.

[8] O. Madelung (Ed.): Semiconductors – Basic Data, Springer-Verlag, Berlin 1996.

[9] B. Sapoval and C. Hermann: Physics of Semiconductors, Springer-Verlag, New York 1995.

[10] A.E. Delahoy, M. Akhtar, J. Bruns, A. Ruppert, L. Chen, and Z. Kiss, "Ternary Source Materials for CIGS Buffer Layers," 16th European Photovoltaic Solar Energy Conference, Glasgow, UK, May 1-5, 2000.

[11] A.E. Delahoy, A.F. Ruppert, and M. Contreras, Thin Solid Films 361-362 (2000) 140-144.

[12] A.E. Delahoy, J.S. Britt, A.M. Gabor, and Z.J. Kiss, AIP Conf. Proc. Vol. 353 (AIP, NY, 1996) pp. 3-11.

[13] M. Powalla, G. Voorwinden and B. Dimmler, 14th European PVSEC (1997) pp. 1270-1273.

[14] B. Dimmler et al., 2nd World Conference on PVSEC (1998) pp. 419-423.

[15] J. Britt, S. Wiedeman, R. Wendt, S. Albright, Phase I Technical Report, Subcontract ZAK-8-17619-04, 1999.

[16] G.M. Hanket, P.D. Paulson, W.N. Shafarman, and R.W. Birkmire, Proc. NCPV Program Review Meeting 2000, pp. 241-242.

Acknowledgments

We gratefully acknowledge the diligent efforts and contributions of the following members of the EPV research, process development, pilot line, and support staff CIGS team:

Masud Akhtar, Malgorzata Bilek, Juergen Bruns, Jeff Camera, Leon Chen, Daniel Chorobski, Alan Delahoy (Principal Investigator), Frank Faras, Barbara Fraczkowska, Zoltan Kiss (Program Manager), Elzbieta Libuda, Rob Lyndall, Agnieszka Pogorzelski, Al Ruppert, Renata Saramak, Frank Sheppard, Krystyna Szewczyk, Howard Tedder, Tony Varvar, Jacek Wisniewski, Frank Ziobro.

The following institutions (and individuals) are also acknowledged for their help and interest:

National Renewable Energy Laboratory (Sally Asher, Miguel Contreras, Rick Matson, Rommel Noufi, Harin Ullal, Ken Zweibel)
Colorado State University (Jim Sites)
University of Illinois (Angus Rockett)
Institute of Energy Conversion/Univ. Delaware (Bob Birkmire, Bill Shafarman)
University of Toledo (Al Compaan)

Thanks are due also to all members of the National CIS Team for their collaborations and discussions.

This work has been largely supported by the US DOE under NREL subcontract ZAK-8-17619-21.

REPORT DOCUMENTATION PAGE

Form Approved
OMB NO. 0704-0188

1. AGENCY USE ONLY (Leave blank)	2. REPORT DATE	3. REPORT TYPE AND DATES COVERED
	August 2000	Annual Technical Report; 16 April 1999-15 April 2000

4. TITLE AND SUBTITLE
Thin Film CIGS Photovoltaic Technology; Annual Technical Report, Phase II; 16 April 1999-15 April 2000

5. FUNDING NUMBERS
C: ZAK-8-17619-21
TA: PV005101

6. AUTHOR(S)
A.E. Delahoy, J. Bruns, A. Ruppert, M. Akhtar, L. Chen, and Z.J. Kiss

7. PERFORMING ORGANIZATION NAME(S) AND ADDRESS(ES)
Energy Photovoltaics, Inc.
P.O. Box 7456
Princeton, NJ 08543

8. PERFORMING ORGANIZATION REPORT NUMBER

9. SPONSORING/MONITORING AGENCY NAME(S) AND ADDRESS(ES)
National Renewable Energy Laboratory
1617 Cole Blvd.
Golden, CO 80401-3393

10. SPONSORING/MONITORING AGENCY REPORT NUMBER
NREL/SR-520-28786

11. SUPPLEMENTARY NOTES
NREL Technical Monitor: H.S. Ullal

12a. DISTRIBUTION/AVAILABILITY STATEMENT
National Technical Information Service
U.S. Department of Commerce
5285 Port Royal Road
Springfield, VA 22161

12b. DISTRIBUTION CODE

13. ABSTRACT *(Maximum 200 words)* A summary of Energy Photovoltaics' Phase II work includes the following:

- EPV has demonstrated that it can sputter a Mo back-contact capable of supporting very high efficiency cell processing. Using EPV Mo, NREL has deposited a 17.1% CIGS cell (no AR coating). EPV believes it can identify the signature of "good" Mo. The Mo was produced on EPV's 0.43 m^2 pilot-line equipment.
- EPV has performed compound synthesis for several classes of materials, namely non-Cu precursor materials, Cu-containing materials, and ternary buffer materials. Using a ternary compound synthesized at EPV (ZIS) as an evaporation source material for the buffer layer, a Cd-free CIGS device has been produced having an efficiency of 11.5% (560 mV, 32.1 mA/cm^2, FF 64.3%). The ZIS films are photoconductive, and the devices exhibit no dark-light crossover or light soaking effects.
- EPV initiated the interest of the University of Oregon in capacitance spectroscopy of CIGS devices. An Urbach tail with characteristic energy E0 < 20meV was identified by transient photocapacitance spectroscopy.
- Small-area CIGS devices were produced in the pilot-line system with an efficiency of 12.0% (581 mV, 30.1 mA/cm^2, FF 68.7%), and in an R&D-scale system with 13.3% efficiency (569 mV, 34.1 mA/cm^2, FF 68.1%).
- An improved linear evaporation source for Cu delivery has been developed and was used for CIGS formation in the pilot-line system. The deposition width is 45 cm. This technological "tour de force" allows EPV to build large-area CIGS systems possessing considerable flexibility. In particular, both EPV's *FORNAX* process and NREL's 3-stage process have been implemented on the pilot line. A CIGS thickness uniformity of ± 7% over a 40 cm width has been achieved.
- A 4-head linear source assembly was designed, constructed, and is in use. Flux monitoring is practiced.
- Large-area CIGS modules were produced with V_{oc}'s up to 36.3 V.
- EPV has started to construct an entirely new CIGS pilot line for scale-up and limited manufacturing purposes. The coating width will be 65 cm.
- The company's analytical capabilities are currently being upgraded with the installation of ICP and SEM/EDS facilities.

14. SUBJECT TERMS
photovoltaics ; Thin-Film Partnership Program ; molybdenum process development ; small-area CIGS ; junction research ; large-area CIGS ; thin-film solar cells; back contact ; Cd-free CIGS device

15. NUMBER OF PAGES

16. PRICE CODE

17. SECURITY CLASSIFICATION OF REPORT	18. SECURITY CLASSIFICATION OF THIS PAGE	19. SECURITY CLASSIFICATION OF ABSTRACT	20. LIMITATION OF ABSTRACT
Unclassified	Unclassified	Unclassified	UL